Optimal Urban Multi-network Coordination Considering Hybrid Pricing Strategy for Electricity and Hydrogen Trading

Cun Zhang, Yifei Wang, Yujian Ye, Qingshan Xu, and Pei Zhang

***Abstract*—The growing demand for optimal urban multi-network coordination has intensified the interdependencies among urban transportation, energy systems, and carbon emissions, with integrated charging stations (ICSs) playing a pivotal role in this interconnected ecosystem. However, optimal coordination across these networks and hybrid pricing strategy for electricity and hydrogen trading remain significant challenges. This paper presents an optimal urban multi-network coordination framework, integrating the urban traffic network (UTN), power distribution network (PDN), urban hydrogen network (UHN), hydrogen supply chain (HSC), ICS, and carbon emission evaluation. The proposed framework aims to maximize regional social welfare, support low-carbon objectives, and optimize multi-network coordination through a two-layer iterative optimization process. Next, a hybrid pricing strategy for electricity and hydrogen trading is introduced, focusing on addressing urban safety constraints. This strategy employs peer-to-peer (P2P) trading for transactions between logistics operators and ICSs. Finally, simulation results on a IEEE 20-node UTN and IEEE 33-node PDN validate the efficiency and accuracy of the proposed framework, demonstrating improvements in multi-network coordination, reductions in traffic congestion and hydrogen transport risks, lower carbon emissions, and enhanced economic performance of both ICSs and central hydrogen production facility (CHPF).**

***Index Terms*—Integrated charging station (ICS), carbon emission, multi-network coordination, urban traffic network (UTN), power distribution network (PDN), hybrid pricing strategy, electricity and hydrogen trading, peer-to-peer (P2P) trading.**

I. INTRODUCTION

HYDROGEN is an efficient power source with non-pollution outgrowth. The raw materials of hydrogen production can be diverse, including water, natural gas, and biomass [1], [2] that are easy to obtain. However, high production costs, infrastructure challenges, and few application scenarios limit the widespread adoption of hydrogen. With the escalating energy crisis and renewable energy advancements in power systems, green hydrogen produced from the electrolytic water has emerged as a promising solution for harnessing renewable energy and mitigating carbon emission [3], [4]. International Renewable Energy Agency (IRENA) predicts that the cost of green hydrogen will drop below $1 per kg by 2050, making green hydrogen more competitive [5]. Besides, National Energy Administration of China has released a medium and long-term plan for the development of the hydrogen industry, promoting the importance of the green hydrogen production. Hydrogen is getting further recognition worldwide as an exclusive energy solution and a potential fuel as it offers carbon-free solutions.

Nowadays, the collaborative development and transformation of urban multi-energy systems is critical in meeting future low-carbon energy needs. Traditionally, urban transportation and energy systems operate independently, with a weak coupling between them. However, with the ongoing advancements in electric and hydrogen energy, the integrated operation of urban traffic networks (UTNs) and electricity and hydrogen systems have become increasingly important. Despite the potential benefits, hydrogen energy safety remains a significant concern, with pipeline transportation posing unpredictable security risks. In urban settings, using road transportation for hydrogen supply presents a viable alternative. Furthermore, challenges related to pricing are introduced. Road transportation requires the consideration of overall time-window demands and transportation costs, which complicates route planning. As a result, the hydrogen supply chain (HSC), particularly the hydrogen network, lacks a grid structure, making it difficult to apply traditional distribution local margin price (DLMP) methods to determine node prices and offer price guidance for integrated charging stations (ICSs). Moreover, in previous research, ICSs have typically been treated as standard facilities, without considering the unique characteristics of their operators. Therefore, there is a need to explore novel methods that not only ensure the profitability of ICSs but also establish an effective hybrid pricing strategy for electricity and hydrogen trading.

The urban hydrogen network (UHN) includes hydrogen

Manuscript received: February 20, 2025; revised: June 9, 2025; accepted: July 22, 2025. Date of CrossCheck: July 22, 2025. Date of online publication: September 5, 2025.

This work was supported by State Grid Corporation of China under Project "Standardization of Flexible Load Response Models for Grid Regulation and Control and Research on Adjustable Margin Prediction Technologies" (No. 5400-202320581A-3-2-ZN).

C. Zhang, Y. Wang (corresponding author), Y. Ye, and Q. Xu are with the School of Electrical Engineering, Southeast University, Nanjing, China (e-mail: cunzhangseu@seu.edu.cn; wyf@seu.edu.cn; yeyujian@seu.edu.cn; xuqingshan@seu.edu.cn).

P. Zhang is with the School of Electrical and Information Engineering, Tianjin University, Tianjin, China (e-mail: peizhang@tju.edu.cn).

DOI: 10.35833/MPCE.2025.000147

production, storage, and transportation. Owing to the intermittent nature of some auspicious renewable energy sources such as solar and wind, hydrogen can take full advantage of renewable energy sources and can be employed as an energy carrier and storage media [6]. Most of the green hydrogen production happens in the hydrogen generation stations (HGSs) near the large-scale renewable energy base. Once hydrogen is produced, its storage presents a complex technological challenge due to the flammable and combustible nature of gas [7]. The hydrogen storage methods include compressed hydrogen, liquefied hydrogen, cryo-compressed hydrogen, physically adsorbed hydrogen, metal hydrides, complex hydrides, and liquid organic hydrogen carrier (LOHC) or liquid organic hydrides [8], which can be roughly divided into gas, liquid, and solid states. The most widely used method for hydrogen storage is the compressed hydrogen at high pressure [9]. It is noted that existing fuel transportation infrastructure that is used for other chemical fuels can also be employed for hydrogen delivery [10]. However, hydrogen transportation through pipelines could be significantly different from natural gas pipeline transportation due to the embrittling effect of hydrogen on pipeline materials, leading to increased transportation costs and safety risks [11]. Currently, the European Union considers only 10% blending of hydrogen with natural gas for pipeline transportation [12]. Thus, hydrogen tube trucks (HTTs) and cryogenic liquid hydrogen trucks have become the most efficient transportation patterns [13]. In this context, the coupling between the HSC and urban traffic network (UTN) is inevitable. The planning path generation of HTTs is similar to the vehicle routing problem (VRP), which involves consumer demand, time-window constraints, and the same objective function for minimizing the travel cost [14]. Day-ahead planning of HTT routines has become a conventional method [15]. With the comprehensive planning of hydrogen production, storage, and transportation, the overall hydrogen industry chain has been optimized.

In terms of the daily operation, single-level optimization for the UHN mainly focuses on the production process and model [16], [17]. Linearization coefficient of the hydrogen production rate can greatly promote the calculation speed, but with less concern of the production constraints [15]. The startup and shutdown states of the electrolytic water device (EWD) can be considered to depict the time-sequential of hydrogen production in detail [18]. Both models consider the renewable energy curtailment that aims to minimize the system cost. In terms of the growing trend of the diverse energy demands in urban areas, the coupling of UHN and power distribution networks (PDNs) has become increasingly tight. The intermittency of renewable energy output prevents the hydrogen production station (HPS) from planless operation [19], [20], where sometimes electricity purchase from the PDN is inevitable to guarantee the hydrogen demand of the consumers. Besides the stand-alone HPS, most grid-connected HPSs take peak-load shifting function [21]. Thus, research on optimizing the interaction between PDN and UTN can significantly reduce the risk of overload in PDN and improve the utilization rate of renewable energy. Most of the bi-level coordinated optimization models of UTN and PDN involve the maximum utilization of renewable energy and safety boundary of the PDN operation [22], [23].

Pricing strategy is another key aspect in guiding orderly hydrogen production and consumption, as well as reducing wind and solar curtailment [24]. Previous studies have utilized the DLMP as the charging price for electric vehicle (EV) users at EV charging stations (EVCSs). In these cases, Karush-Kuhn-Tucker (KKT) conditions [25] are introduced to transform the dual-layer structure into a single layer, reducing the computational burden of multi-network coordination. Additionally, demand response-based pricing strategies have also been applied to EV charging [26], [27]. Besides, hydrogen pricing plays a critical role in integrated electricity and hydrogen systems, where market design and renewable variability heavily influence cost formation. Studies show that flexible electrolysis aligned with low electricity prices can reduce hydrogen production costs, though initial underutilization may lead to higher prices before market maturity [28], [29]. In local energy markets, hydrogen can be traded alongside electricity, with prices shaped by real-time supply-demand dynamics. A Shapley value-based profit allocation method is applied in [30], assuming short-term fixed hydrogen prices within local integrated markets. Reference [31] introduces an iterative clearing mechanism where hydrogen prices reflect both trading bids and external hydrogen station prices. Additionally, high transportation and storage costs may significantly raise end-use hydrogen prices, emphasizing the importance of local production [29]. Despite the progress, further research is needed to model dynamic hydrogen pricing under uncertainties of policy and infrastructure. Therefore, it is imperative to explore new pricing strategies to determine hydrogen node prices and optimize both transportation and energy distribution.

The energy replacement process in urban areas can significantly lower carbon emission levels. However, congestion in the UTN may delay arrival time and increase carbon emissions, as many drivers tend to leave their engines running during traffic jams [32]. Additionally, the waste of renewable energy and the over-reliance on thermal power plants exacerbate carbon emissions [33]. Therefore, an effective method for carbon emission evaluation is crucial. Energy-carbon integrated prices [34]-[36], recognized as an efficient method to promote low-carbon behavior, can optimize power generation and distribution. However, the multi-network coupling and coordination become increasingly complex due to flexible demand and the need for coordination across different timescales. Reference [37] proposes a novel low-carbon EV charging coordination method for coupled transportation and power networks, formulated as a bi-level optimization problem. Flow tracing of carbon emission is adopted to compute rational locational-differentiated price signals, demonstrating an effective price incentive mechanism for low-carbon coordination in the UTN under uncertain traffic conditions. Nevertheless, the coordination with the UHN, which is a crucial component for achieving zero-carbon goals, has yet to be adequately addressed in existing research.

In conclusion, the holistic modeling method facilitates the coordinated optimization of urban multi-networks, effectively addressing significant challenges in system modeling complexity and computational tractability. First, the coupling relations of the UTN, PDN, UHN, HSC, ICS, and carbon emission evaluation remain unknown, which makes the feasible region of urban multi-network coordination unclear. ICSs, as the most important hub connecting UTN, PDN, UHN, HSC, and carbon emission evaluation, cannot be simply regarded as mere energy replenishment facilities. They can also have a significant impact on urban traffic flow and load distribution through pricing strategies. Second, the hybrid pricing strategy for electricity and hydrogen trading, which involves numerous internal and external cost factors, still requires a feasible solution. The hydrogen pricing strategy differs significantly from the electricity pricing strategy, which can be derived through DLMP. The road-based HSC involves traffic conditions, hydrogen production, and distance, which can possibly impact the hydrogen pricing strategy. Finally, the research of carbon emission in the multi-network coupling is insufficient. The carbon emissions, which include the vehicle output in the UTN, the distributed generation in the PDN, the congestion level of the UTN, etc., have not been sufficiently studied. The method of evaluating the carbon emissions and analysis of their impact on the operation optimization could be complex and imprecise. Therefore, there is a need to develop a suitable framework that can optimize the multi-network coupling operation and provide feasible hybrid pricing strategy for electricity and hydrogen trading for the ICS operators, so as to ensure the low-carbon emission and cross the barriers of severe model nonlinearity and non-convexity.

In order to close the research gap, this paper proposes an optimal urban multi-network coordination framework. By analyzing all the coupling relations between the different components, the proposed framework induces a set of feasible solutions that can effectively meet the demand, while considering the interactions between electricity and hydrogen trading, thereby ensuring efficient and sustainable system operation. The contributions of this paper are threefold.

1) An optimal urban multi-network coordination framework is proposed that integrates UTN, PDN, UHN, HSC, ICS, and carbon emission evaluation. The proposed framework enables coordinated scheduling across these components, improving efficiency, reducing operation costs, and promoting carbon emission reduction.

2) An urban multi-network coordination model is developed to capture the interdependencies of UTN, PDN, UHN, HSC, ICS, and carbon emission evaluation. The proposed model facilitates optimized energy distribution, hydrogen logistics, and traffic flow management, offering a unified solution for urban multi-network coordination.

3) A novel hybrid pricing strategy for electricity and hydrogen trading is proposed, combining peer-to-peer (P2P) trading for hydrogen with DLMP-based electricity pricing. The proposed strategy enhances resource allocation efficiency and supports low-carbon goals by optimizing the operation of both electricity and hydrogen markets.

The rest of this paper is structured as follows. Section II presents the optimal urban multi-network coordination framework. The urban multi-network coordination model is presented in Section III. The hybrid pricing strategy for electricity and hydrogen trading is presented in Section IV. Section V presents the case study, and Section VI concludes the paper.

II. Optimal Urban Multi-network Coordination Framework

Figure 1 illustrates the decomposition of the proposed framework structured into the upper layer and lower layer. In Fig. 1, DG is short for distributed generation, and DT is short for delivery truck. The proposed framework aims to coordinate the operation of the UTN, PDN, and UHN through a hybrid pricing strategy for electricity and hydrogen trading. Note that the detailed example of real-world map can be observed in Supplementary Material A.

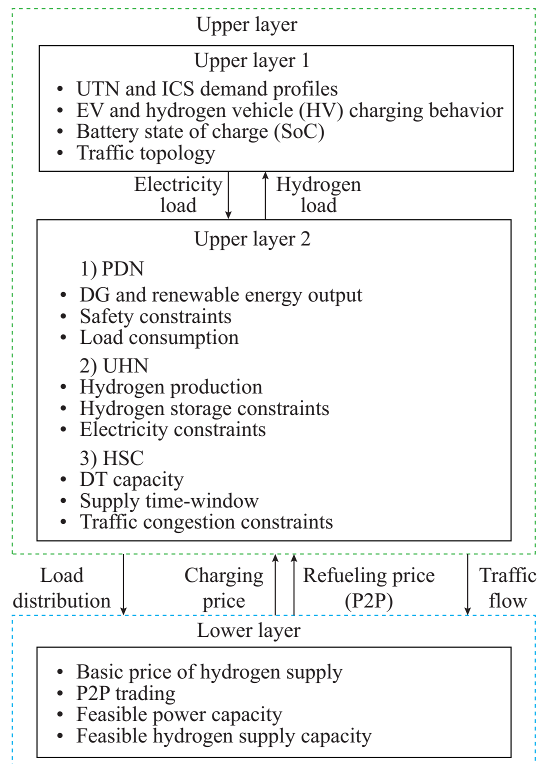

Fig. 1. Decomposition of proposed framework.

The upper layer is further divided into two sublayers. Upper layer 1 focuses on the demand side, including the UTN and ICS demand profiles, EV and HV charging behavior, battery SoC, and traffic topology. This sublayer captures the spatio-temporal demand patterns of both electricity and hydrogen. Upper layer 2 addresses the supply-side and system constraints, covering the PDN, UHN, and HSC. Specifically, it considers DG and renewable energy output, safety constraints, and load consumption for PDN; hydrogen production, hydrogen storage constraints, and electricity constraints for UHN; and DT capacity, supply time-window, and traffic congestion constraints for HSC. Together, these elements define feasible operation regions for electricity and hydrogen supply.

The lower layer integrates market signals and operation feasibility. It determines load distribution, charging price, refueling price under P2P trading, and traffic flow. This layer also accounts for the basic price of hydrogen supply, P2P trading, feasible power capacity, and feasible hydrogen supply capacity. In this way, the lower layer establishes the market-operation interaction, enabling coordinated decisions across the coupled systems.

In conclusion, the proposed framework is a bi-level problem with nest loops, which has never been considered in existing research.

III. Urban Multi-network Coordination Model

The proposed model outlined in this section includes the UTN model, PDN model, UHN model with HSC, ICS model, and carbon emission evaluation model.

A. UTN Model

In the UTN model, gasoline vehicles (GVs), EVs, and HVs constitute the primary components of the traffic flow. The energy charging process for GVs is not discussed in this paper. The charging behaviors and durations for EVs and HVs differ, requiring them to charge or refuel in ICSs, which leads to an optimal distribution of electric and hydrogen loads. The optimal traffic flow model is derived using the modified user equilibrium-traffic assignment problem (UE-TAP) [11], [17]. The linearization method can be observed in [17], which allows for the determination of load distribution and the congestion levels across the links, which is not the main contribution of this paper. The objective function of UTN model is given by:

$$\min\left[\omega_e\sum_{a\in A}t_a\left(x_{ae}\right)\iota_{ae}^{w}+\sum_{k\in K}\left(\omega_e t_{ke}\left(x_{ke}\right)\iota_{ke}^{w}+\lambda_{ke}^{SP}f_{ke}^{p,w}\right)+\omega_h\sum_{a\in A}t_a\left(x_{ah}\right)\iota_{ah}^{w}+\sum_{k\in K}\left(\omega_h t_{kh}\left(x_{kh}\right)\iota_{kh}^{w}+\lambda_{kh}^{SP}f_{kh}^{p,w}\right)\right] \tag{1}$$

where a and A are the index and set of links of UTN, respectively; k and K are the index and set of ICSs, respectively; ω_e and ω_h are the unit time costs of EV and HV, respectively; x_{ae} and x_{ah} are the traffic flows of EV and HV, respectively; x_{ke} and x_{kh} are the traffic flows of EV and HV, respectively; λ_{ke}^{SP} and λ_{kh}^{SP} are the charging and refueling prices, respectively; $f_{ke}^{p,w}$ and $f_{kh}^{p,w}$ are the traffic flows of EV and HV on origin-destination (OD) pair w in path p, respectively; t_a is the time function; ι_{ae}^{w} and ι_{ah}^{w} are the binary variables indicating whether EV and HV are on OD pair w, respectively; t_{ke} and t_{kh} are the time functions of EV and HV, respectively; and ι_{ke}^{w} and ι_{kh}^{w} are the binary variables indicating whether EV and HV on OD pair w pass ICS k, respectively. λ_{ke}^{SP} equals the dual multiplier λ_i^{E} of PDN, and λ_{kh}^{SP} can be calculated through the energy trading. The UTN model can deliver electricity and hydrogen loads to the PDN and UHN, and deliver traffic flow to the HSC and carbon emission evaluation for further optimization and evaluation.

B. PDN Model

After the electricity load is obtained by UTN model, the power flow distribution over PDN is generally obtained by solving the alternating current optimal power flow (ACOPF) problem, which is non-convex and NP-hard. Pursuing tractability, convex relaxation is performed, resulting in the formulation of the second-order cone programming (SOCP) problem. The formulation of PDN model is expressed as:

$$\min\left[\sum_{i\in DG}\left(c_i^{l}\left(P_i^{DG}\right)^2+c_i^{q}P_i^{DG}\right)+\sigma P^{DRS}\right] \tag{2}$$

s.t.

$$P_{i,j}-r_{i,j}I_{i,j}+P_i^{N}=\sum P_{j,i}\quad \forall j \tag{3}$$

$$Q_{i,j}-x_{i,j}I_{i,j}+Q_i^{N}=\sum Q_{j,i}\quad \forall j \tag{4}$$

$$P_i^{N}=P_i^{DG}+P_i^{DR}+P_i^{BY}-P_i^{D}-P_i^{EV}-P_i^{RN,h}\quad \forall i \tag{5}$$

$$Q_i^{N}=Q_i^{DG}-Q_i^{D}\quad \forall i \tag{6}$$

$$P_i^{DR}=P_i^{DRG}-P_i^{DRS}\quad \forall i \tag{7}$$

$$U_i-U_j=-2\left(r_{j,i}P_{j,i}+x_{j,i}Q_{j,i}\right)+\left(r_{j,i}+x_{j,i}\right)^2 I_{j,i}\quad \forall i,\forall j \tag{8}$$

$$I_{i,j}U_i\geq P_{i,j}^2+Q_{i,j}^2\quad \forall i,\forall j \tag{9}$$

$$\sqrt{P_{i,j}^2+Q_{i,j}^2}\leq S_{i,j}^{Line}\quad \forall i,\forall j \tag{10}$$

$$U_{i,\min}\leq U_i\leq U_{i,\max}\quad \forall i \tag{11}$$

$$P_{i,\min}^{DG}\leq P_i^{DG}\leq P_{i,\max}^{DG}\quad \forall i \tag{12}$$

$$Q_{i,\min}^{DG}\leq Q_i^{DG}\leq Q_{i,\max}^{DG}\quad \forall i \tag{13}$$

where i and j are the indexes of PDN nodes; DG is the set of PDN nodes; $P_{i,j}$ and $Q_{i,j}$ are the active and reactive power flows of line (i,j), respectively; P_i^{DRS} and P_i^{DRG} are the spillage amount and total amount of distributed renewable generator (DRG) in PDN, respectively; σ is the penalty coefficient for the spillages of DRG; c_i^{l} and c_i^{q} are the linear and quadratic cost coefficients of DG, respectively; U_i is the voltage; P_i^{D} and Q_i^{D} are the active and reactive power of residential load, respectively; $r_{i,j}$ and $x_{i,j}$ are the resistance and reactance of line (i,j), respectively; $I_{i,j}$ is the square of the current of line (i,j); $S_{i,j}^{Line}$ is the allowable maximum apparent power of the line (i,j); P_i^{DR} is the DRG consumption; P_i^{BY} is the active power purchased from the upper grid; P_i^{EV} is the active power of EV; $P_i^{RN,h}$ is the active power for hydrogen production; P_i^{DG} and Q_i^{DG} are the active and reactive power of DG, respectively; P_i^{N} and Q_i^{N} are the active and reactive power in PDN, respectively; and subscripts min and max represent the low and upper bounds of corresponding variables, respectively.

The objective function (2) combines the cost of the DG and the punishment of renewable energy spillage. Constraints (3) and (4) present the node active and reactive power balances for each PDN nodes, respectively. Constraints (5) and (6) represent the node net active and reactive power generation, respectively, where the load of the EV charging is obtained by the UTN model. Constraint (7) expresses the usage of the renewable energy at PDN node. Constraint (8) describes the voltage magnitude drop for each line, while constraint (9) performs the second-order cone relaxation.

Constraints (10) and (11) represent the thermal and square voltage magnitude limits, respectively. Constraints (12) and (13) detail the minimum and maximum limits for active and reactive power output of DG, respectively. Additionally, the load of the UHN and ICS should also be concluded and will be discussed in the following sections.

C. UHN Model with HSC

The UHN model with HSC mainly includes hydrogen production, storage, and delivery. Due to financial and safety concerns, the central hydrogen production facility (CHPF) should be built near the renewable energy station and adopt the power of renewable energy priorly. The model of hydrogen production at CHPF node h, l_h^{elw}, is expressed as:

$$l_h^{elw}=\frac{\eta^{elz}p_h^{RN,h}}{LHV} \tag{14}$$

where η^{elz} is the efficiency of electrolyzing water; and LHV is a constant value. The hydrogen production process is time-varying which does not match the 5-15 min dispatching time of the power grid. For simplicity, it is assumed that the average production rate of hydrogen remains unchanged during the dispatching period.

The constraint of hydrogen storage is:

$$\frac{U^{tank}}{R^{gas}T^{tank}}\left(e^{tank}-e_0^{tank}\right)=l^{elw}-l^{out} \tag{15}$$

where R^{gas} is the gas constant of hydrogen; U^{tank} and T^{tank} are the volume and temperature of hydrogen storage tank, respectively; e^{tank} is the pressure of hydrogen storage tank; e_0^{tank} is the original pressure of hydrogen storage tank; and l^{out} is the output of hydrogen storage tank.

The capacity of hydrogen storage tank at CHPF u^{tank} can be expressed as:

$$u^{tank}=u_0^{tank}+\left(l^{elw}-l^{out}\right) \tag{16}$$

where u_0^{tank} is the original capacity of hydrogen storage tank at CHPF. After the hydrogen is produced, it needs to be liquefied before being transported. Considering the low temperature of liquid hydrogen storage tank and the pressure requirements, safety constraints can be concluded as:

$$e_{\min}^{tank}\le e^{tank}\le e_{\max}^{tank} \tag{17}$$

$$u_{\min}^{tank}\le u^{tank}\le u_{\max}^{tank} \tag{18}$$

$$0\le l^{elw}\le l_{\max}^{elw} \tag{19}$$

Since the hydrogen load includes the ICS refueling demand and industrial loads, the total hydrogen load can be expressed as:

$$\sum_{v\in HLS}L_v^{load}=\sum_{v\in HLS}L_v^{industrial}+\sum_{v\in HLS}L_v^{ICS} \tag{20}$$

$$sum\left(l^{out}\right)=sum\left(L_v^{load}\right) \tag{21}$$

where v represents the hydrogen load node in UTN, which belongs to HLS index, i.e., HLS; and L_v^{load}, $L_v^{industrial}$, and L_v^{ICS} are the hydrogen loads for total hydrogen load, industrial hydrogen load, and HV refueling load in ICSs, respectively. Constraint (21) represents that the CHPF output should equal the hydrogen demand. The objective function of UHN model is given by:

$$\min F^{CHPF}=\sum_{h\in H}\lambda_h^{BY}P_h^{BY} \tag{22}$$

where F^{CHPF} is the cost of the CHPF purchased from the upper grid; H is the set of CHPF nodes; and λ_h^{BY} is the electricity price purchased by CHPF from the upper grid. For most of the research, hydrogen is transported through the natural gas pipeline, which we think is a big safety hidden trouble for the urban area. Thus, the hydrogen transportation in this paper, i.e., the HSC, is through DT. The HSC model can be referred in [23]. Note that the price of the CHPF is added as the constraint in the HSC, which is expressed as:

$$\min F^{HSC}=\sum_{t\in T}\alpha^{DT}T^{arr} \tag{23}$$

where F^{HSC} is the total cost of HSC; α^{DT} is the unit cost of DT; t and T are the index and set of time periods, respectively; and T^{arr} is the arrival time of DT for delivery task. Equation (23) will be added to the objective function to minimize HSC costs, thereby obtaining the price of CHPF transportation for participating in P2P trading. The linearization method can be observed in [23].

D. ICS Model

After modeling the urban multi-network is modelled, the model of the energy sellers in the urban area should also be considered. The ICSs are the facilities that can sell electricity and hydrogen together. The ICSs in this paper can be sorted into two categories, i.e., the central integrated charging station (CICS) and the normal integrated charging station (NICS). The differences between CICS and NICS are the trading permission and the facilities, where the CICS has the same character as the virtual power plant (VPP) and can trade hydrogen and electricity to other NICSs. ICSs can provide the energy charging service for EVs and HVs. The basic model can be observed in [37], which will not be discussed in this paper.

E. Carbon Emission Evaluation Model

After all the optimization processes are completed, the carbon emissions of the multi-network should be evaluated. In the urban area, the source of carbon emission can be diversified, which is mainly devoted by the vehicles in the UTN and the power source of the PDN. DG in the urban area can be regarded as the thermal power plant. The formulation of carbon emission of the thermal power plant $E_{CO_2}^{DG}$ can be expressed as:

$$E_{CO_2}^{DG}=\gamma_{CO_2}^{DG}\sum_{i=1}^{N}P_i^{DG} \tag{24}$$

where $\gamma_{CO_2}^{DG}$ is the carbon emission coefficient of DG; and N is the total number of DG nodes.

The electricity purchased (or bought, denoted by the superscript BY) from the upper grid is regarded as the same as the carbon emission from the thermal power plant, which can be expressed as:

$$E_{CO_2}^{BY}=\gamma_{CO_2}^{BY}\sum_{i=1}^{N}P_i^{BY} \tag{25}$$

In this paper, the carbon emission for renewable energy in the power plant and the integrated energy system is regarded as zero. Thus, the total carbon emission of PDN with integrated energy system $E_{CO_2}^{PDN}$ can be expressed as:

$$E_{CO_2}^{PDN}=E_{CO_2}^{DG}+E_{CO_2}^{BY} \tag{26}$$

Besides, the UTN also devotes most of the carbon emission due to the vehicles. The carbon emission of GV $E_{CO_2}^{GV}$ can be expressed as:

$$E_{CO_2}^{GV}=\frac{\gamma_{CO_2}^{GV}D}{\eta^{ICE}} \tag{27}$$

where η^{ICE} is the carbon emission transfer coefficient of internal combustion engine (ICE) in GV; $\gamma_{CO_2}^{GV}$ is the carbon emission coefficient of GV; and D is the total distance that the vehicles pass.

The carbon emission of EV $E_{CO_2}^{EV}$ can be expressed as:

$$E_{CO_2}^{EV}=\frac{\gamma_{CO_2}^{EV}DP^{EV}}{\eta^{EM}} \tag{28}$$

where $\gamma_{CO_2}^{EV}$ is the carbon emission coefficient of EV; η^{EM} is the carbon emission transfer coefficient of electric motor (EM) in EV; and P^{EV} is the electricity consumed by the EVs during the journey to their destination. Since the renewable energy is considered with zero carbon emission, P^{EV} should be further converted to the adjusted EV electricity consumption for carbon emission calculation $\tilde{P}^{EV}$, which is expressed as:

$$\tilde{P}^{EV}=\frac{P^{EV}\sum_{i=1}^{N}P_i^{DG}}{\sum_{i=1}^{N}P_i} \tag{29}$$

where P_i is the total electricity consumed by the multi-networks. Equation (29) represents the carbon emissions solely attributed to the DG output (including the battery storage, etc.). Moreover, the traffic congestion can produce more carbon emissions due to the engine still being activated. Thus, the total carbon emission of UTN $E_{CO_2}^{UTN}$ should be modified as:

$$E_{CO_2}^{UTN}=E_{CO_2}^{GV}+E_{CO_2}^{EV}+E_{CO_2}^{Congestion} \tag{30}$$

$$E_{CO_2}^{Congestion}=\frac{\gamma_{CO_2}^{Congestion}\sum_{a=1}^{N}t_a}{\sum_{a=1}^{N}t_{a0}} \tag{31}$$

where $E_{CO_2}^{Congestion}$ is the carbon emission caused by traffic congestion; t_{a0} is the free flow time of link a; and $\gamma_{CO_2}^{Congestion}$ is the carbon emission coefficient of the traffic congestion. The total carbon emission $E_{CO_2}^{Total}$ in this paper is expressed as:

$$E_{CO_2}^{Total}=E_{CO_2}^{PDN}+E_{CO_2}^{UTN} \tag{32}$$

With the formulations above, the carbon emission in the urban area can be obtained.

IV. Hybrid Pricing Strategy for Electricity and Hydrogen Trading

Pricing plays a key role in aligning the coordination of the multi-network by influencing energy distribution, demand response, and traffic flow. By adjusting prices, the proposed framework can effectively balance the supply and demand of electricity and hydrogen, ensure optimal resource allocation, and foster smooth collaboration of UTN, PDN, and UHN with HSC.

A. Hybrid Pricing Strategy for Hydrogen

In the past, hydrogen network calculations typically determine the hydrogen price through pipeline modeling, with hydrogen energy being transported via pipelines by default. However, in practice, due to the embrittlement effect of hydrogen on pipelines and safety concerns, the use of highway hydrogen transport is considered more promising. This method avoids the pipeline-related risks, offering a more flexible and safer transport solution. There is no fixed path for the HSC, and the optimal path needs to be determined through a collaborative evaluation of road operations, hydrogen load demand at each road node, and hydrogen production status. Such a problem is akin to the VRP, where the optimal routes need to be identified dynamically based on these factors. In this paper, hydrogen procurement is divided into multiple channels. The first is the purchase from CHPF in PDN. The characteristics of such facilities are well-defined, and hydrogen production is influenced by the synergistic effect of new energy, regional hydrogen demand, and economic factors. The second is the ICS within the region, which is abundant in renewable energy sources. These stations not only meet their own energy demands but also serve as energy retailers, providing supplemental energy to other ICSs in the area.

CHPF is the main hydrogen provider in the urban area, where all the ICSs can purchase hydrogen from the CHPF. In this paper, the CHPF is assumed to be the same company as the ICSs, which means the hydrogen price of the CHPF only depends on the logistics cost. The logistics cost $\lambda_{u,v}^{CHPF}$ can be divided into two aspects, which are the basic cost for the distance $\lambda_{u,v}^{CHPF,base}$ and the risk cost $\lambda_{u,v}^{CHPF,risk}$ for the congestion on the links.

$$\lambda_{u,v}^{CHPF}=\lambda_{u,v}^{CHPF,base}+\lambda_{u,v}^{CHPF,risk} \tag{33}$$

$$\lambda_{u,v}^{CHPF,base}=\alpha^{CHPF,base}\sum_{u,v\in VRP,u\neq v}D_{u,v}^{travel} \tag{34}$$

where $\alpha^{CHPF,base}$ is the basic unit cost coefficient of CHPF; u and VRP represent the node index and set of routes obtained by VRP, respectively; u,v represents the delivery route segment starting from node u and ending at node v; and $D_{u,v}^{travel}$ is the travel distance. Note that $D_{u,v}^{travel}$ can be obtained by the VRP simulation result.

$\lambda_{u,v}^{CHPF,risk}$ can be expressed as:

$$\lambda_{u,v}^{CHPF,risk}=\sum_{u,v\in VRP,u\neq v}\frac{t_a(u,v)}{t_{a0}(u,v)} \tag{35}$$

The larger the $\lambda_u^{CHPF,risk}$, the higher the risk level for hydrogen transportation exploration.

Besides the CHPF, some ICSs in the urban area can also provide hydrogen for the other ICSs due to the coordination production of HPF and facilities in ICSs. ICSs that have the abilities and are authorized to sell the hydrogen are referred to as the CICS, while the other ICSs are the NICS. Thus, the hydrogen trading in the urban area has become a hybrid attribute hydrogen-trading model that considers the hydrogen supply cost and P2P bidding. The formulation of the objective function is:

$$\max \sum_{u=1}^{IS}\sum_{v=1}^{NICS}\lambda_{u,v}^{P2P}L_{u,v}^{NICS} \tag{36}$$

where $\lambda_{u,v}^{P2P}$ is the P2P trading cost; IS is the total number of the CHPFs and CICSs; $NICS$ is the total number of NICSs; and $L_{u,v}^{NICS}$ is the trading hydrogen of NICS, which should follow constraint (37).

$$L_{u,v}^{NICS}=\sum_{h=1}^{CHPF}LS_{hu,v}^{CHPF}+\sum_{v=1}^{CICS}LS_{u,v}^{CICS} \tag{37}$$

where hu,v represents the hydrogen delivery from CHPF node h at node u to node v; $LS_{hu,v}^{CHPF}$ is the hydrogen traded from the CHPF; $CHPF$ and $CICS$ are the total numbers of CHPFs and CICSs, respectively; and $LS_{u,v}^{CICS}$ is the hydrogen that can be purchased from CICS.

Besides constraint (37), the constraint for P2P trading should also be stated as:

$$\sum_{u=1}^{NIS}L_{u,v}^{NICS}\leq LS_{hu,v}^{CHPF}+LS_{u,v}^{CICS} \tag{38}$$

where NIS is the total number of NISs.

Constraint (38) denotes that the hydrogen demand in the urban area should be less than the hydrogen production in the urban area. The formulation for the hydrogen that can be purchased from the CICS is expressed as:

$$LS_{u,v}^{CICS}=\sum_{hu=1}^{CICS}\left(LP_{u}^{CICS}+LS_{hu,v}^{CHPF}-LL_{u}^{CICS}\right) \tag{39}$$

where LP_{u}^{CICS} is the hydrogen production for CICS; and LL_{u}^{CICS} is the hydrogen consumption for CICS.

Based on the principle of profit maximization, NICSs can choose to sell hydrogen directly or retain inventory and trade it when prices rise. For social welfare purposes, CICSs are required to fully cover regional hydrogen demand and supply reserved hydrogen to make up for insufficient supply from NICSs, as expressed by:

$$\sum_{u=1}^{CICS}LS_{u,v}^{CICS}\geq LL_{v}^{NICS} \tag{40}$$

where LL_{v}^{NICS} is the hydrogen consumption for NICS. The hydrogen traded by NICSs should also be positive.

$$L_{u}^{NICS}\geq 0 \tag{41}$$

Additionally, constraint (42) should be followed, which means hydrogen demand for ICS LL_{u}^{ICS} equals the sum of LL_{u}^{CICS} for CICS and hydrogen demand for NICS, i.e., LL_{u}^{NICS}.

$$LL_{u}^{ICS}=LL_{u}^{CICS}+LL_{u}^{NICS} \tag{42}$$

Moreover, the P2P price of CICS $\lambda_{u,v}^{CICS}$ should also be divided into two parts as:

$$\lambda_{u,v}^{CICS}=\lambda_{u,v}^{CICS,base}+\lambda_{u,v}^{CICS,bid} \tag{43}$$

$$\lambda_{u,v}^{CICS,base}=\alpha^{CICS,base}\sum_{u\neq i,u\in VRP}D_{u,v}^{travel} \tag{44}$$

where $\lambda_{u,v}^{CICS,base}$ is the basic hydrogen trading cost from CICS; and $\alpha^{CICS,base}$ is the unit cost of hydrogen supply route; and $\lambda_{u,v}^{CICS,bid}$ is the bidding price of CICS, which is derived from the pricing curve, and can also be applied to other pricing strategy. Thus, the pricing strategy of P2P λ_{u}^{P2P} can be expressed as:

$$\lambda_{u}^{P2P}=\left\{\lambda_{u,v}^{CHPF},\lambda_{u,v}^{CICS}\right\} \tag{45}$$

From the constraints above, the formulation of the hybrid pricing strategy for the hydrogen can be obtained as:

$$\begin{cases}\max \sum_{u=1}^{IS}\sum_{v=1}^{NIS}\lambda_{u}^{P2P}L_{u}^{NICS}\\ \text{s.t. } (33)\text{-}(35),\ (37)\text{-}(45)\end{cases} \tag{46}$$

With the formulation above, the hydrogen price for each ICS can be obtained. In this paper, each station can realize the behavior of purchasing and selling hydrogen through its own strategies. Moreover, hydrogen can also be delivered between stations through trading to reduce the pressure of CHPF and avoid the losses caused by the high procurement cost of distant ICSs or the loss of users caused by the increase of hydrogen selling price.

B. Pricing Strategy for PDN

The pricing strategy for PDN could be varied including the P2P trading, P2P bidding, etc, which has been discussed in many other research works and is not the main contribution of this paper. In this paper, the PDN price is obtained through the dual multiplier of (3), which can reflect the electricity load distribution and is regarded as the pricing strategy for the ICSs. Besides the formulations above, the linear method can be observed in Supplementary Material B.

V. Case Studies

A. Parameters of UTN and PDN with UHN

The case studies of this paper are through the simulation of multi-networks. IEEE 20-node UTN and IEEE 33-node PDN with their coupling relation are shown in the Supplementary Material C Fig. SC1 and Tables SCI-SCIII. All the simulation is calculated on an i7-13700k, 32 GB RAM desktop. The mode is coded in MATLAB 2021a with YALMIP toolbox and solved by Gurobi.

B. Different Cases for Proposed Framework

The diversification of energy supply and demand in the urban areas leads to the main reason for the changeable distribution of the traffic flow and charging behavior. Three different cases are designed to validate the efficiency and the performance of the proposed framework.

1) Case 1

In case 1, no P2P trading is involved and CHPF is the sole provider of hydrogen for all ICSs, indicating the absence of other competitors in the area. The ICSs function solely as energy suppliers. The iterative process terminates after five rounds, including the final validation iteration. The traffic flow on each link for case 1 before and after price optimization is illustrated in Fig. 2. As shown in Fig. 2, the congestion on several links is reduced, while some links experience more severe congestion due to their proximity to the origin points of the OD pairs. The effectiveness of the price incentive mechanism in directing traffic flow is evident. To better illustrate this effect, the congestion levels for the links and ICSs in case 1 are presented in Fig. 3.

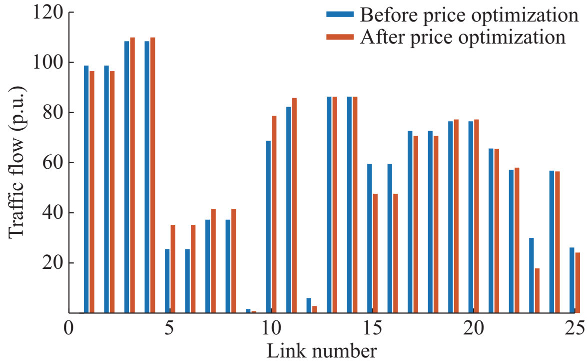

Fig. 2. Traffic flow on each link for case 1 before and after price optimization.

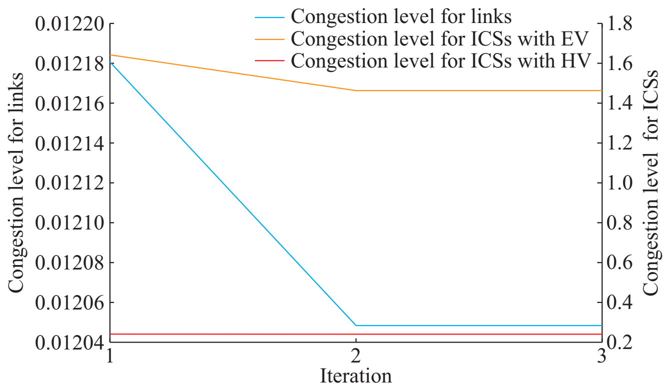

Fig. 3. Congestion levels for links and ICSs in case 1.

As shown in Fig. 3, the congestion levels for links and ICSs with EV are higher than that for ICSs with HV due to the scale. Moreover, the congestion level for ICSs with EV is reduced at each iteration due to the guidance of the pricing strategy. Additionally, the calculation results of charging and refueling in ICSs for case 1 are presented in Table I, where P^{ev}, λ^e, L^{HV}, and λ^h are the EV charging power, EV charging price, HV refueling quality, and HV refueling price, respectively.

TABLE I
CALCULATION RESULTS OF CHARGING AND REFUELING IN ICSS FOR CASE 1

ICS number	P^{ev} (kW)	λ^e ($/kWh)	L^{HV} (kg)	λ^h ($/kWh)
1	900.000	1.371	220.000	1.293
2	777.893	1.370	217.447	1.000
3	710.000	1.365	182.012	1.600
4	900.000	1.363	214.703	0.733
5	525.744	1.359	220.000	0.733
6	513.000	1.363	94.553	1.533
7	669.362	1.381	219.999	0.933
8	475.500	1.394	220.000	1.227

As shown in Table I, most ICSs have reached their upper charging and refueling limits due to the influence of traffic flow and varying prices. The disparity of λ^h is greater than that of λ^e, primarily due to the absence of a hydrogen network and route selection by HSC. The costs of the multi-network coordination for case 1 are detailed in Table II.

TABLE II
COSTS OF MULTI-NETWORK COORDINATION FOR CASE 1

Item	Cost after 1st iteration (10^4 $)	Cost after 2nd iteration (10^4 $)	Cost after 3rd iteration (10^4 $)
UTN	1785.986	1211.168	1213.506
PDN-UHN	627.982	628.478	628.478
ICS	159.323	158.872	158.872

As shown in Table II, the costs of the UTN and PDN-UHN decrease after three iterations. The total earnings of the ICSs initially increase slightly but then decrease due to price fluctuations. Overall, the simulation results align well with the expectations of the objective function.

2) Case 2

P2P trading is included in case 2. CHPF and CICSs collaboratively support the hydrogen supply in the urban area. CICSs operate as VPPs, trading the hydrogen within the P2P trading framework. The renewable energy output in the VPPs is set to be 120 kW and 60 kW, respectively. The iterative process converges after four iterations, with the final iteration used for result verification. The traffic flow on each link for case 2 before and after price optimization is illustrated in Fig. 4.

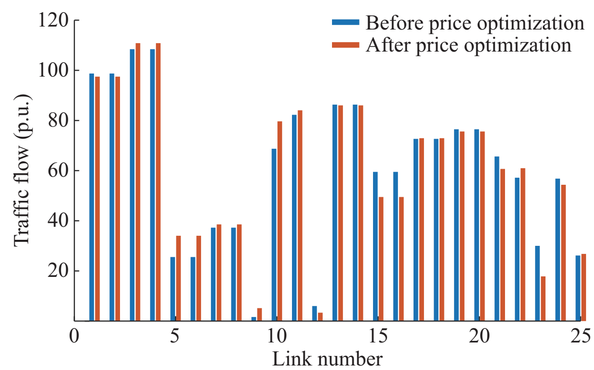

Fig. 4. Traffic flow on each link for case 2 before and after price optimization.

As shown in Fig. 4, the traffic flow results in case 2 differ slightly from those in case 1, indicating that traffic saturability has reached a very high level. The congestion levels for links and ICSs in case 2 are presented in Fig. 5.

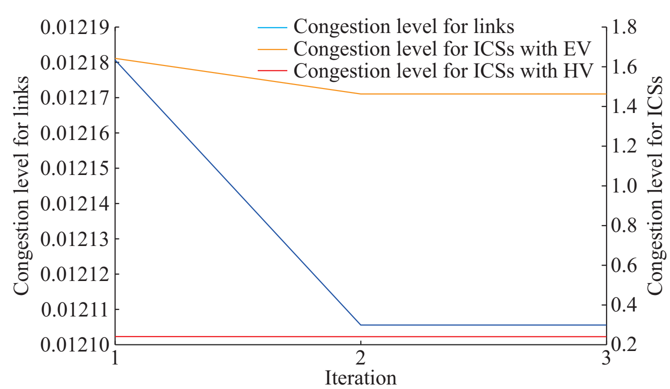

Fig. 5. Congestion levels for links and ICSs in case 2.

As shown in Fig. 5, the congestion levels in case 2 show a notable increase compared with those in case 1. However, the congestion level for ICSs with EV remains nearly unchanged due to the consistency of electricity trading. In case 2, the available renewable energy is sufficient to meet all the demands, which means that P2P trading can help lower the congestion level for ICSs. The calculation results of charging and refueling for ICSs in case 2 are presented in Table III.

TABLE III
CALCULATION RESULTS OF CHARGING AND REFUELING FOR ICSS IN CASE 2

ICS number	P^{ev} (kW)	λ^e (\$/kWh)	L^{HV} (kg)	λ^h (\$/kWh)
1	900.000	1.371	220.000	1.533
2	777.893	1.370	220.000	1.167
3	710.000	1.365	220.000	2.000
4	900.000	1.363	220.000	0.917
5	525.744	1.359	220.000	0.917
6	513.000	1.363	73.339	2.000
7	669.362	1.381	220.000	1.167
8	475.500	1.394	220.000	1.533

As can be observed in Table III, the results of P^{ev} and λ^e are the same as those in case 1, while the results of L^{HV} and λ^h are larger than those in case 1 due to the participation of the P2P trading. Note that the results of L^{HV} are larger than those in case 1, which is not an error of the function. High λ^h will prompt HV users to carefully select their refueling options and avoid refueling at ICSs with high prices unless necessary. ICS2 is the necessary station where most HVs must pass. Thus, HV would choose to refuel in ICS2 rather than ICSC6 with the same λ^h, since ICS6 is far from most of the OD destination. The hydrogen provided by CHPF and CICSs can be observed in Supplementary Material C Fig. SC2. The costs of multi-network coordination for case 2 can be observed in Table IV.

TABLE IV
COSTS OF MULTI-NETWORK COORDINATION FOR CASE 2

Iterm	Cost after 1st iteration (10^4 \$)	Cost after 2nd iteration (10^4 \$)	Cost after 3rd iteration (10^4 \$)
UTN	1785.986	1218.610	1222.921
PDN-UHN	628.817	628.774	628.774
ICS	159.323	161.334	161.334

As shown in Table IV, the costs of the UTN and ICS in case 2 are slightly higher than those in case 1, primarily due to that the P2P trading among ICSs increases the operation cost. This trading allows ICSs to generate higher profits, while HVs are incentivized to reach their destinations without over-refueling. Besides, the cost of the PDN-UHN slightly increases, as the energy selling prices of refueling in case 2 are higher than those in case 1.

3) Case 3

Case 3 includes the P2P trading. The hydrogen production from CHPF is insufficient due to facility breakdowns or a lack of renewable energy from distant sources. As a result, the CICSs become the primary hydrogen providers, effectively demonstrating the advantages of this type of VPP. The traffic flow on each link in case 3 before and after price optimization is illustrated in Fig. 6.

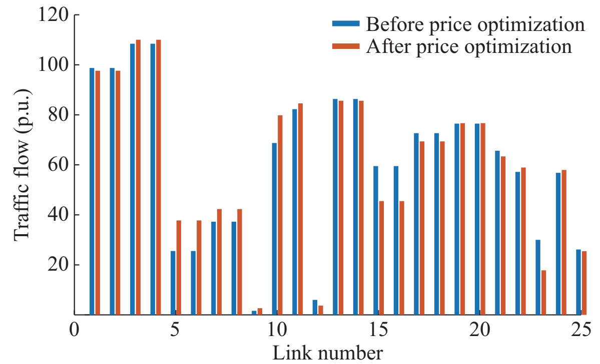

Fig. 6. Traffic flow on each link in case 3 before and after price optimization.

As shown in Fig. 6, the traffic flow results differ slightly from those in the previous cases, with variations observed on a few links such as links 23 and 24 that have a minimal impact on the overall multi-networks. The congestion levels for links and ICSs in case 3 are presented in Fig. 7.

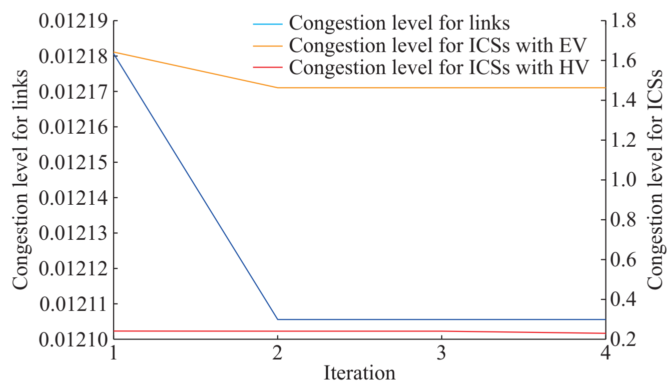

Fig. 7. Congestion levels for links and ICSs in case 3.

As shown in Fig. 7, the congestion levels for links and ICSs remain consistent with those in case 2 due to the unchanged charging and refueling demands. The calculation results of charging and refueling for ICSs in case 3 are provided in Table V. As shown in Table V, the results of L^{HV} in case 3 are reduced, especially in ICS5 and ICS6. This reduction is mainly attributed to the limited hydrogen supply from CHPF, which elevates reliance on the CICSs while increasing the volatility of hydrogen prices. Nevertheless, the results highlight the resilience of the CICS-based VPP mechanism, which ensures system continuity under constrained supply conditions, albeit with higher refueling costs and uneven price distribution. In certain ICSs, the refueling prices are significantly higher, which is attributed to their strategic locations, as HVs cannot reach their destinations without refueling in these ICSs. The hydrogen provided by the CHPF and ICSs is presented in Supplementary Material C Fig. SC3. The costs of multi-network coordination in case 3 are detailed in Table VI.

TABLE V
CALCULATION RESULTS OF CHARGING AND REFUELING FOR ICSs IN CASE 3

ICS number	P^{ev} (kW)	λ^e (\$/kWh)	L^{HV} (kg)	λ^h (\$/kWh)
1	900.000	1.371	220.000	1.045
2	777.893	1.370	220.000	2.053
3	710.000	1.365	220.000	1.437
4	900.000	1.363	220.000	1.803
5	525.744	1.359	132.951	1.033
6	513.000	1.363	141.336	2.109
7	669.362	1.381	220.000	1.320
8	475.500	1.394	218.782	1.687

TABLE VI
COSTS OF MULTI-NETWORK COORDINATION IN CASE 3

Item	Cost after 1st iteration (10^4 \$)	Cost after 2nd iteration (10^4 \$)	Cost after 3rd iteration (10^4 \$)	Cost after 4th iteration (10^4 \$)
UTN	1785.986	1217.995	1220.525	1218.215
PDN-UHN	135.441	135.494	135.485	135.473
ICS	159.323	161.334	161.334	161.334

As shown in Table VI, the costs of the UTN and ICS exhibit minimal differences between cases 1 and 2, while the cost of the PDN-UHN significantly decreases due to that the cost of the HSC could be far less than the electricity purchased from the upper grid. These results highlight the crucial support function of VPPs in urban areas.

C. Carbon Emission Comparison in Different Cases

The carbon emission coefficients of DG, EV, GV, and congestion level are 25.8 gCO_2/kWh, 0.107 gCO_2/m, 2.9251 gCO_2/m, and 0.5 gCO_2/s, respectively. The comparison of carbon emission amount of cases 1-3 before and after price optimization is presented in Table VII.

TABLE VII
COMPARISON OF CARBON EMISSION AMOUNT IN CASES 1-3 BEFORE AND AFTER PRICE OPTIMIZATION

Case	Carbon emission amount (kg)		
	Before price optimization	After price optimization	Difference
1	7936.9496	7917.2930	−19.6566
2	7936.9496	7901.0634	−35.8862
3	8671.0394	8655.6927	−15.3466

The carbon emissions per minute in the urban area are significantly reduced with the integration of CICSs. As shown in Table VII, while case 3 exhibits the highest absolute carbon emissions, it also demonstrates the largest reduction in carbon emissions due to the extensive utilization of renewable energy within the CICSs, which means the CICSs provide the electricity for PDN. This indicates that CICSs effectively leverage renewable energy sources to offset emissions, even in scenarios with high initial emissions. Besides the total carbon emission, the proportion of different parts for the carbon emissions has also been calculated. The proportion of carbon emissions from each component can be obtained based on (24)-(32) by dividing the carbon emission of each part by the total carbon emissions. The emission profile in cases 1 and 2 is dominated by congestion related sources (65%). GV emissions make up 24%, followed by EV emissions at 8% and DG emissions at 3%. These results indicate that inefficient traffic flow and vehicle idling are the primary sources of carbon emissions, with relatively low contributions from the energy system side. The minimal share of DG suggests limited reliance on DG in this scenario. In contrast, case 3 exhibits a significantly different emission profile. The congestion and DG each account for 40% of total emissions, while GV emissions fall to 14% and EV emissions decline modestly to 6%. This shift demonstrates that the participation of CICSs in P2P hydrogen trading effectively mitigates traffic-related emissions but introduces higher dependency on DG, highlighting a trade-off between transport-side and energy-side carbon emission reduction.

Overall, the transition from cases 1 and 2 to case 3 reflects a notable improvement in traffic-side carbon emissions, yet the increase in DG emissions underscores the need for further integration of renewable energy sources to avoid carbon leakage. These findings validate the effectiveness of the proposed framework in enhancing multi-network coordination, optimizing traffic and energy operations, and promoting carbon emission reduction in urban areas.

The results highlight that the integration of CICSs can substantially lower carbon emission levels in urban areas across various conditions, reinforcing the importance of incorporating CICSs into urban multi-network coordination to achieve sustainability goals and mitigate environmental impacts.

The case studies validate the proposed framework and strategy across three cases. In case 1, traffic congestion is alleviated to a certain extent, but the hydrogen price variance among ICSs remains high due to uncoordinated logistics and inflexibility. In contrast, case 2 enhances flexibility and economic efficiency. This leads to more balanced hydrogen distribution, mitigated congestion in ICSs, and improved profit margins, while enabling load-responsive price differentiation. In case 3, CICSs serve as vital backup providers, demonstrating strong resilience and supporting system continuity with minimal impact on traffic dynamics. Although this case yields higher dependence on DG, the overall framework still achieves carbon emission reduction through better traffic flow and localized usage of renewable energy.

Quantitatively, total carbon emissions decrease by 19.66 kg, 35.89 kg, and 15.35 kg in cases 1-3, respectively, with congestion consistently being the dominant emission source. Case 3 shows a shift in emission composition, i.e., DG emissions rise due to reduced CHPF capacity, but emissions from congestion and GVs fall significantly. These results highlight the ability of the proposed framework to adaptively balance traffic and energy emissions, maintain profitability, and respond to renewable intermittency.

VI. Conclusion

This paper presents a novel framework to optimize urban multi-network coordination by integrating the UTN, PDN, UHN, HSC, and carbon emission evaluation. The proposed hybrid pricing strategy for electricity and hydrogen trading, particularly the P2P trading strategies, has shown significant effectiveness in reducing carbon emissions and improving the overall efficiency of the proposed framework. The case studies demonstrate how this framework not only optimizes traffic flow but also enhances the coordination between multi-network, especially through the role of CICSs, which lead to substantial carbon emission reductions.

The findings emphasize the practical importance of integrating multi-network, highlighting how the proposed strategy can reduce congestion, optimize hydrogen distribution, and promote low-carbon solutions. Future research will focus on refining the method to ensure global optimality, as well as integrating real-time data analytics to enhance the adaptability of the system in dynamic urban environments. Moreover, expanding the model to include additional energy carriers, such as thermal energy or natural gas, and incorporating multiple transportation modes, will provide a more comprehensive and robust solution for achieving urban sustainability and supporting decarbonization efforts.

References

[1] V. A. Panchenko, Y. V. Daus, A. A. Kovalev *et al*., "Prospects for the production of green hydrogen: review of countries with high potential," *International Journal of Hydrogen Energy*, vol. 48, no. 12, pp. 4551-4571, Feb. 2023.

[2] A. M. Nasrabadi and M. Korpeh, "Techno-economic analysis and optimization of a proposed solar-wind-driven multigeneration system; case study of Iran," *International Journal of Hydrogen Energy*, vol. 48, no. 36, pp. 13343-13361, Apr. 2023.

[3] A. V. Vorontsov and P. G. Smirniotis, "Advancements in hydrogen energy research with the assistance of computational chemistry," *International Journal of Hydrogen Energy*, vol. 48, no. 40, pp. 14978-14999, May 2023.

[4] W. Zhou, S. Chen, X. Meng *et al*., "Energy-saving cathodic H2 production enabled by non-oxygen evolution anodic reactions: a critical review on fundamental principles and applications," *International Journal of Hydrogen Energy*, vol. 48, no. 42, pp. 15748-15770, May 2023.

[5] International Renewable Energy Agency. (2025, Mar.). Renewable capacity statistics 2025. [Online]. Available: https://www.irena.org

[6] H. Ishaq, I. Dincer, and C. Crawford, "A review on hydrogen production and utilization: challenges and opportunities," *International Journal of Hydrogen Energy*, vol. 47, no. 62, pp. 26238-26264, Jul. 2022.

[7] S. W. Jorgensen, "Hydrogen storage tanks for vehicles: recent progress and current status," *Current Opinion in Solid State and Materials Science*, vol. 15, no. 2, pp. 39-43, Apr. 2011.

[8] M. R. Usman, "Hydrogen storage methods: review and current status," *Renewable and Sustainable Energy Reviews*, vol. 167, p. 112743, Oct. 2022.

[9] F. Zhang, P. Zhao, M. Niu *et al*., "The survey of key technologies in hydrogen energy storage," *International Journal of Hydrogen Energy*, vol. 41, no. 33, pp. 14535-14552, Sept. 2016.

[10] H. J. Yoon, S. K. Seo, and C. J. Lee, "Multi-period optimization of hydrogen supply chain utilizing natural gas pipelines and byproduct hydrogen," *Renewable and Sustainable Energy Reviews*, vol. 157, p. 112083, Apr. 2022.

[11] U.S. Department of Energy. (2024, Jan.) HyBlend: opportunities for hydrogen blending in natural gas pipelines. [Online]. Available: https://www.nrel.gov/aries/

[12] G. He, D. S. Mallapragada, A. Bose *et al*., "Hydrogen supply chain planning with flexible transmission and storage scheduling," *IEEE Transactions on Sustainable Energy*, vol. 12, no. 3, pp. 1730-1740, Jul. 2021.

[13] M. E. Demir and I. Dincer, "Cost assessment and evaluation of various hydrogen delivery scenarios," *International Journal of Hydrogen Energy*, vol. 43, no. 22, pp. 10420-10430, May 2018.

[14] Y. Pu, Q. Li, S. Luo *et al*., "Peer-to-peer electricity-hydrogen trading among integrated energy systems considering hydrogen delivery and transportation," *IEEE Transactions on Power Systems*, vol. 39, no. 2, pp. 3895-3911, Mar. 2024.

[15] C. Feng, C. Shao, Y. Xiao *et al*., "Day-ahead strategic operation of hydrogen energy service providers," *IEEE Transactions on Smart Grid*, vol. 13, no. 5, pp. 3493-3507, Sept. 2022.

[16] Y. Du, X. Shen, B. Lu *et al*., "Joint optimization of layout and electrolyzer capacity for decentralized offshore wind-powered hydrogen production," *IEEE Transactions on Industrial Informatics*, vol. 21, no. 5, pp. 4158-4168, May 2025.

[17] H. Khajeh, S. Seyyedeh-Barhagh, and H. Laaksonen, "Optimized operation of hybrid wind-hydrogen system to provide flexibility for transmission system needs," *IEEE Transactions on Sustainable Energy*, vol. 16, no. 3, pp. 1576-1588, Dec. 2024.

[18] G. Pan, W. Gu, Y. Lu *et al*., "Optimal planning for electricity-hydrogen integrated energy system considering power to hydrogen and heat and seasonal storage," *IEEE Transactions on Sustainable Energy*, vol. 11, no. 4, pp. 2662-2676, Oct. 2020.

[19] A. Ali, M. F. Shaaban, and K. Mahmoud, "Optimizing hydrogen systems and demand response for enhanced integration of RES and EVs in smart grids," *IEEE Transactions on Smart Grid*, vol. 16, no. 2, pp. 1366-1378, Mar. 2025.

[20] X. Lai, J. Yang, F. Wen *et al*., "Operational economics of renewable energy-hydrogen system with hydrogen-powered transportation," *IEEE Transactions on Smart Grid*, vol. 16, no. 1, pp. 718-727, Jan. 2025.

[21] C. Shao, C. Feng, M. Shahidehpour *et al*., "Optimal stochastic operation of integrated electric power and renewable energy with vehicle-based hydrogen energy system," *IEEE Transactions on Power Systems*, vol. 36, no. 5, pp. 4310-4321, Sept. 2021.

[22] Z. Wang, L. Zhou, L. Xiong *et al*., "Voltage-source control for green-hydrogen hybrid energy storage system with operational constraints and current rate limiter," *IEEE Transactions on Smart Grid*, vol. 16, no. 4, pp. 2871-2883, Jul. 2025.

[23] K. Zhang, B. Zhou, C. Y. Chung *et al*., "A coordinated multi-energy trading framework for strategic hydrogen provider in electricity and hydrogen markets," *IEEE Transactions on Smart Grid*, vol. 14, no. 2, pp. 1403-1417, Mar. 2023.

[24] S. P. Singh and S. Padmanaban, "Prosumer energy management for optimal utilization of bid fulfillment with EV uncertainty modeling," *IEEE Transactions on Industry Applications*, vol. 58, no. 1, pp. 599-611, Jan. 2022.

[25] C. Shao, K. Li, T. Qian *et al*., "Generalized user equilibrium for coordination of coupled power-transportation network," *IEEE Transactions on Smart Grid*, vol. 14, no. 3, pp. 2140-2151, May 2023.

[26] Y. Cui, Z. Hu, and X. Duan, "A multi-period charging service pricing game for public charging network operators considering the dynamics of coupled traffic-power systems," *IEEE Transactions on Intelligent Transportation Systems*, vol. 24, no. 9, pp. 9355-9367, Sept. 2023.

[27] Y. Li, M. Han, Z. Yang *et al*., "Coordinating flexible demand response and renewable uncertainties for scheduling of community integrated energy systems with an electric vehicle charging station: a bi-level approach," *IEEE Transactions on Sustainable Energy*, vol. 12, no. 4, pp. 2321-2331, Oct. 2021.

[28] P. Hesel, S. Braun, F. Zimmermann *et al*., "Integrated modelling of European electricity and hydrogen markets," *Applied Energy*, vol. 328, p. 120162, Dec. 2022.

[29] P. Mochi, K. A. Espegren, and M. Korpås, "Short communication: local electricity-hydrogen market," *International Journal of Hydrogen Energy*, vol. 116, pp. 17-22, Apr. 2025.

[30] J. Zhu, D. Meng, X. Dong *et al*., "An integrated electricity-hydrogen market design for renewable-rich energy system considering mobile hydrogen storage," *Renewable Energy*, vol. 202, pp. 961-972, Jan. 2023.

[31] Y. Xiao, X. Wang, P. Pinson *et al*., "A local energy market for electricity and hydrogen," *IEEE Transactions on Power Systems*, vol. 33, no. 4, pp. 3898-3908, Jul. 2018.

[32] G. Liu, Y. Tao, Z. Ge *et al*., "Data-driven carbon footprint management of electric vehicles and emission abatement in electricity networks," *IEEE Transactions on Sustainable Energy*, vol. 15, no. 1, pp. 95-108, Jan. 2024.

[33] Y. Cheng, N. Zhang, B. Zhang *et al*., "Low-carbon operation of multiple energy systems based on energy-carbon integrated prices," *IEEE Transactions on Smart Grid*, vol. 11, no. 2, pp. 1307-1318, Mar. 2020.

[34] X. Wei, Y. Xu, H. Sun *et al*., "Day-ahead optimal dispatch of a virtual power plant in the joint energy-reserve-carbon market," *Applied Energy*, vol. 356, p. 122459, Feb. 2024.

[35] L. Sang, Y. Xu, and H. Sun, "Encoding carbon emission flow in energy management: a compact constraint learning approach," *IEEE Transactions on Sustainable Energy*, vol. 15, no. 1, pp. 123-135, Jan. 2024.

[36] Q. Yuan, Y. Ye, Y. Tang *et al*., "Low carbon electric vehicle charging coordination in coupled transportation and power networks," *IEEE Transactions on Industry Applications*, vol. 59, no. 2, pp. 2162-2172, Mar. 2023.

[37] C. Zhang, Z. Chen, and Q. Guo, "Research on optimal operation strategy of regional multi-heterogeneous energy charging station considering bi-direction satisfaction and traffic network coupling," *Sustainable Energy*, *Grids and Networks*, vol. 37, p. 101259, Mar. 2024.

Cun Zhang received the B. Eng. degree in School of Automation from Guangdong University of Technology, Guangzhou, China, in 2017, and the M.S degree from Nanjing Normal University, Nanjing, China, in 2021. He is currently pursuing the Ph.D. degree at Southeast University, Nanjing, China. His research interests include complex system modeling and analysis, and integrated energy optimization

Yifei Wang received the M.Sc. degree in electrical engineering from Wuhan University, Wuhan, China, and the Ph. D. degree in electrical engineering from Zhejiang University, Hangzhou, China. He is currently an Associate Professor with the School of Electrical Engineering, Southeast University, Nanjing, China. He was a Postdoc with the Electrical and Computer Engineering Department, Illinois Institute of Technology, Chicago, USA. His research interests include convex optimization and artificial intelligence (AI) in power system.

Yujian Ye received the B.Eng. (Hons.) degree from Northumbria University, Newcastle Upon Tyne, U. K., in 2011, and the M. Sc. and Ph. D. degrees from Imperial College London, London, U.K., in 2013 and 2017, respectively. He performed postdoctoral research also with Imperial College London from 2016 to 2020, and then joined Southeast University, Nanjing, China, with Associate Professorship in 2021. He is currently a Professor with Young Endowed Chair Honor with the School of Electrical Engineering at Southeast University and an Honorary Lecturer at Imperial College London. His research interests include development and application of novel data analytics and artificial intelligence techniques in low-carbon energy-transportation-information system modeling, analysis and control, and optimization of economics of power system operation and planning.

Qingshan Xu received the B.S. degree from Southeast University, Nanjing, China, in 2000, the M.S. degree from Hohai University, Nanjing, China, in 2003, and the D.E. degree from Southeast University, in 2006, all in electrical engineering. From 2007 to 2008, he was a Visiting Scholar and cooperated with the Aichi Institute of Technology, Toyota, Japan. He is currently a Professor with the Department of Electrical Engineering, Southeast University. His research interests include renewable energy and power system control.

Pei Zhang received the Ph. D. degree from Imperial College of Science, Technology and Medicine, London, U.K.. He is a Professor at Tianjin University, Tianjin, China. His research interests include power system planning and operation including reliability assessment, stability and control, system restoration, risk assessment, and application of AI technology in power system.